Atomic Magnetometers for Electromagnetic Induction Imaging

Boris Baudel

Ecole normale supérieure de Rennes, France

Pr. Ferruccio Renzoni

University College London, United Kingdom

Abstract

Electromagnetic induction imaging (EMI) uses ultra-sensitive atomic magnetometers (AM), specifically radio-frequency atomic magnetometers (RF-AM). These devices are capable of detecting oscillating magnetic fields, making them ideal for EMI applications. The study aims to take experimental values for high-resolution EMI systems for various materials, focusing on the sensitivity and frequency range of the magnetic sensors including image and signal processsing.

Introduction

A single-channel rubidium RF-AM is used, operating at room temperature with a sensitivity of 55 fT/Hz and a linewidth of 36 Hz, covering the kHz-MHz band. The results demonstrate high-resolution EMI on materials with conductivities ranging from 6.107 Sm-1 to 500 Sm-1, with sample volumes of a few cm³ and an imaging resolution of around 1 mm. The document also details data processing techniques using Matlab to fit Lorentzian models to spectral data and image processing techniques to enhance imaging details [1].
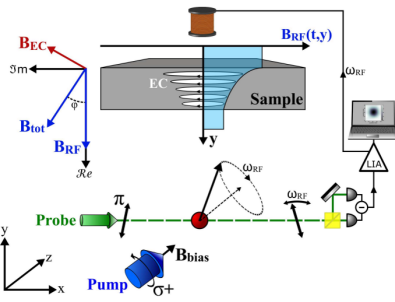

Figure 1: Electromagnetic induction imaging with an atomic magnetometer

Methods

An unshielded radio frequency-modulated atomic magnetometer (RF-AM) setup, based on the initial design by Savukov et al. (2005) [8] is utilized. At the core of the device there is an alkali vapor cell containing rubidium (Rb), which is spin-polarized through optical pumping using a circularly polarized pump beam and a parallel DC magnetic field (bias field - BBIAS). The operating frequency of the RF-AM is adjusted via Helmholtz coils controlling the bias field, leveraging the Zeeman effect to suit the intended application. The magnetometer is calibrated using a known AC magnetic field, which induces a transverse atomic polarization rotation, measured by the rotation of the polarization of a linearly polarized probe beam that crosses the pump beam perpendicularly. Detection is performed by a polarimeter equipped with a polarizing beam splitter and a balanced photodiode, with data analyzed using a lock-in amplifier and a spectrum analyzer. [1]
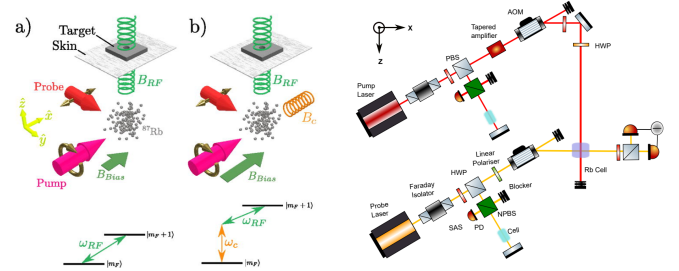

Figure 2: Two photon probe configuration [7]

Figure 3: Probe and pump light path for D1 and D2 transitions

In the setup described, the polarimeter, which consists of a polarizing beam splitter and a balanced photodiode (*Thorlabs PDB210A*), functions to detect the rotation of polarization in the probe beam. The rotation signal detected by the photodiode is then analyzed using a lock-in amplifier (*LIA, Ametek 7280 DSP*) and a spectrum analyzer (*SA, Anritsu MS2718B*). The LIA processes the signal to extract four key streams of data: the in-phase (absorptive, labeled as X) and out-of-phase (dispersive, labeled as Y) components of the polarimeter's output. Additionally, it calculates the radius $R = \sqrt{X^2 + Y^2}$ and the phase $\Phi = \arctan\left(\frac{Y}{X}\right)$. These outputs ($X$, Y, R, and Φ) along with the spectral traces from the SA are then recorded on a laptop for further analysis and interpretation [1] [2].

The given algorithm outlines a method for fitting Lorentzian curves to data points for interpreting magnetic resonance signals. The algorithm processes multidimensional input data and applies Lorentzian and derivative models to each pixel performing least-squares optimization.. This allows for a detailed analysis of the lineshapes of the transverse spin components, represented as $\tilde{S}_x$ and $\tilde{S}_y$, in a magnetic field. The Lorentzian lineshape

for the $\tilde{S}_x$ component is described by the formula:

$$\tilde{S}_x(\omega_{\text{RF}}) = S_0 B_{\text{RF}} \gamma \frac{\Gamma}{4[(\omega_{\text{RF}} - \Omega_L)^2 + \Gamma^2/4]},$$

which is centered on the Larmor frequency Ω_L with a linewidth Γ indicating the system's sensitivity. This response is crucial for determining the properties of the magnetic field by analyzing the detected frequency shifts [1][2]. Similarly, the dispersive component, $\tilde{S}_y$, which provides complementary information about the magnetic field dynamics, is given by:

$$\tilde{S}_y(\omega_{\text{RF}}) = S_0 B_{\text{RF}} \gamma \frac{(\Omega_L - \omega_{\text{RF}})}{2[(\omega_{\text{RF}} - \Omega_L)^2 + \Gamma^2/4]},$$
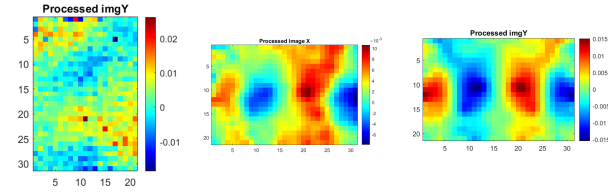

Figure 4: Raw data, Gaussian filtering with $\sigma = 1$, and image with gradient remover function
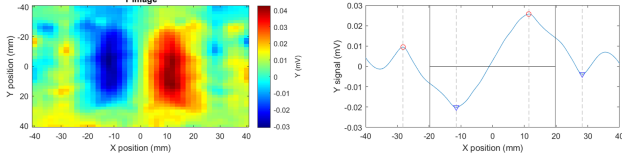

Figure 5: Two holes distance results for the second data set : 36,5mm

The Gaussian filter smooths or blurs an image by applying a convolution with a Gaussian function, reducing noise while preserving overall structures in figure 4. The degree of smoothing is controlled by the standard deviation σ, with larger σ leading to more blurring. Convolution, used to apply filters, combines the image and filter through summation of their products. An algorithm can be developed to calculate the distance between two holes, figure 5 , tested using a small magnetometer, figure 6, on target data [1][2][3].
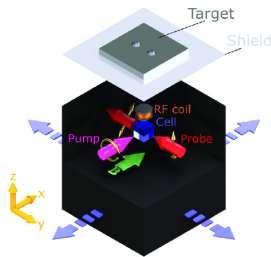

Figure 6: Portable atomic magnetometer [4]

The described experimental conditions involve a 300 MHz Single Path Probe and Single Path Pump, operating in an environment controlled using optical modulation via Acousto-Optic Modulators (AOMs). RF sensitivity setting include a field strength of 2.05×10^{-12}. An additional RF parameter set at 0.1. The AOM for the pump is adjusted to 1.4 volts, and for the probe, it is set slightly higher at 1.6 volts in figure 3. These voltages control the modulation of laser beams used in each path, affecting the frequency, intensity, and directionality of the lasers via sound waves generated within the AOM. We are operating at a temperature of 100 degrees Celsius.

Results

In the two-photon configuration, two RF photons with distinct polarizations are employed. This method exploits the principle that π-polarized RF photons induce π transitions, whereas σ-polarized photons facilitate σ transitions. The scheme incorporates an additional RF field, B_c, which propagates along B_{Bias} and enables a two-photon transition at a designated frequency. The interaction of the σ-polarized B_{RF} photon with the π-polarized B_c photon satisfies the selection rule $\Delta m = \pm 1$, thereby coupling adjacent magnetic sublevels. By tuning ω_c, the RF-AM resonance can be effectively shifted relative to ω_{RF}, without modifying B_{Bias}. The Rabi frequency for this two-photon transition retains the linearity in Ω_{RF} characteristic of the standard RF-AM setup, but incorporates an additional factor [7].
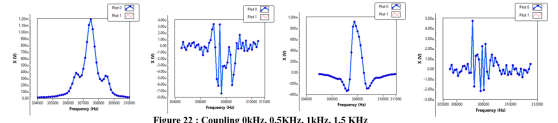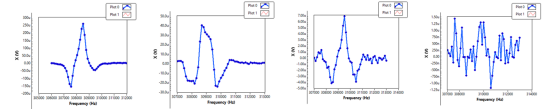

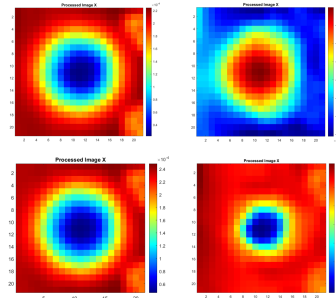Figure 7: Two photon transition on pump results for different coupling frequencies

Figure 8: Experimental results of imaging for a copper coin

The intensity and spread of the eddy currents, as represented in the images, should correlate well with the physical dimensions of the coin [5]. Results from the study highlight a two-photon configuration using RF photons of distinct polarizations to induce precise magnetic transitions. Optimizing the system's performance across varied parameters for a simple photon to reach an RF sensitivity of 2.05×10^{-12}.

Bibliography

[1] Deans, C. (2018). *Electromagnetic Induction Imaging with Atomic Magnetometers.* Doctoral dissertation, University College London, Department of Physics and Astronomy.

[2] Yao, H. (2023). *High-sensitivity unshielded radio-frequency atomic magnetometers.* Doctoral dissertation, University College London, Department of Physics and Astronomy.

[3] Deans, C., Marmugi, L., Hussain, S., Renzoni, F. (2016). *Electromagnetic induction imaging with a radio-frequency atomic magnetometer.* Applied Physics Letters, 108(10):103503. doi:10.1063/1.4943659.

[4] Marmugi, L., Gori, L., Hussain, S., Deans, C., Renzoni, F. (2017). *Remote detection of rotating machinery with a portable atomic magnetometer.* Applied Optics, 56(3):743–749. doi:10.1364/AO.56.000743.

[5] Deans, C., Marmugi, L., Renzoni, F. (2017). *Through-barrier electromagnetic imaging with an atomic magnetometer.* Optics Express, 25(15):17911–17917. doi:10.1364/OE.25.017911.

[6] Deans, C., Marmugi, L., Renzoni, F. (2018). *Active underwater detection with an array of atomic magnetometers.* Applied Optics, 57(10):2346–2351. doi:10.1364/AO.57.002346.

[7] Maddox, B., Renzoni, F. (2023). *Two-photon electromagnetic induction imaging with an atomic magnetometer.* Applied Physics Letters, 122(14). doi:10.1063/5.0147291.

[8] I. M. Savukov, S. J. Seltzer, M. V. Romalis, and K. L. Sauer. *Tunable atomic magnetometer for detection of radio-frequency magnetic fields.* Physical Review Letters, 95(6):063004, 2005. doi:10.1103/PhysRevLett.95.063004.